

Theo yêu cầu của khách hàng, trong một năm qua, chúng tôi đã dịch qua 16 môn học, 34 cuốn sách, 43 bài báo, 5 sổ tay (chưa tính các tài liệu từ năm 2010 trở về trước) Xem ở đây

**DỊCH VỤ
DỊCH
TIẾNG
ANH
CHUYÊN
NGÀNH
NHANH
NHẤT VÀ
CHÍNH
XÁC
NHẤT**

Chỉ sau một lần liên lạc, việc dịch được tiến hành

Giá cả: có thể giảm đến 10 nghìn/1 trang

Chất lượng: Tao dựng niềm tin cho khách hàng bằng công nghệ 1. Bạn thấy được toàn bộ bản dịch; 2. Bạn đánh giá chất lượng. 3. Bạn quyết định thanh toán.

Tài liệu này được dịch sang tiếng việt bởi:

www.mientayvn.com

Xem thêm các tài liệu đã dịch sang tiếng Việt của chúng tôi tại:

http://mientayvn.com/Tai_lieu_da_dich.html

Dịch tài liệu của bạn:

http://mientayvn.com/Tim_hieu_ve_dich_vu_bang_cach_doc.html

Tìm kiếm bản gốc tại đây:

https://drive.google.com/drive/folders/1Zjz7DM7W4iV1qojox5kc_UUiNpx2qSHR?usp=sharing

Nonlinear light scattering from clusters and single particles

Hiệu ứng tán xạ ánh sáng phi tuyến từ các đám hạt và từ các hạt đơn lẻ

Abstract

We present sum-frequency-scattering experiments on colloidal dispersions with various concentrations and in different scattering geometries. At small scattering angles, large fluctuations are observed in the intensity of the scattered sum-frequency photons. By considering the angular dependence of the signal, the particle concentration dependence, and the surface vibrational spectra of the particle, we have determined that the fluctuations are caused by scattering from clusters of particles. We further demonstrate that dynamic nonlinear light scattering may be used to measure the size of the correlated particle clusters.

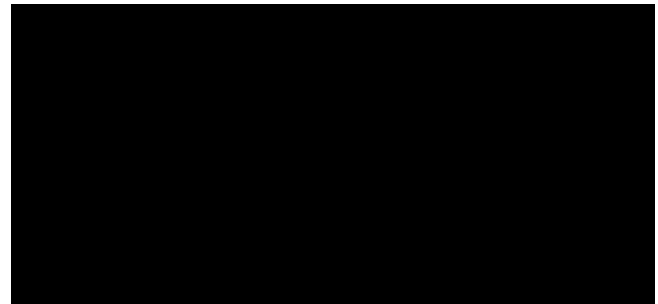
I. INTRODUCTION

For the past four decades, second-order nonlinear optical measurements such as Second-Harmonic Generation (SHG) and Sum-Frequency Generation (SFG) have been used to probe the planar surfaces of materials whose bulk media are centrosymmetric (see e.g. [1-7]). The interface sensitivity of these techniques arises from the fact that within the dipole approximation, SHG or SFG is forbidden from the bulk of centrosymmetric media. At the interface, however, the inversion symmetry is broken thereby allowing the SHG and SFG processes.

Although second harmonic light scattering was observed in a surface-enhanced Hyper-Raman scattering experiment in 1982 [8], it has been performed only with the aim of directly measuring surface properties in 1996 via surface SHG scattering [9]. Within the

Tóm tắt

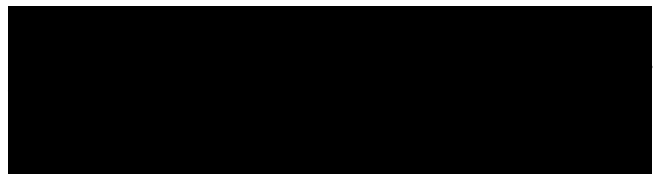
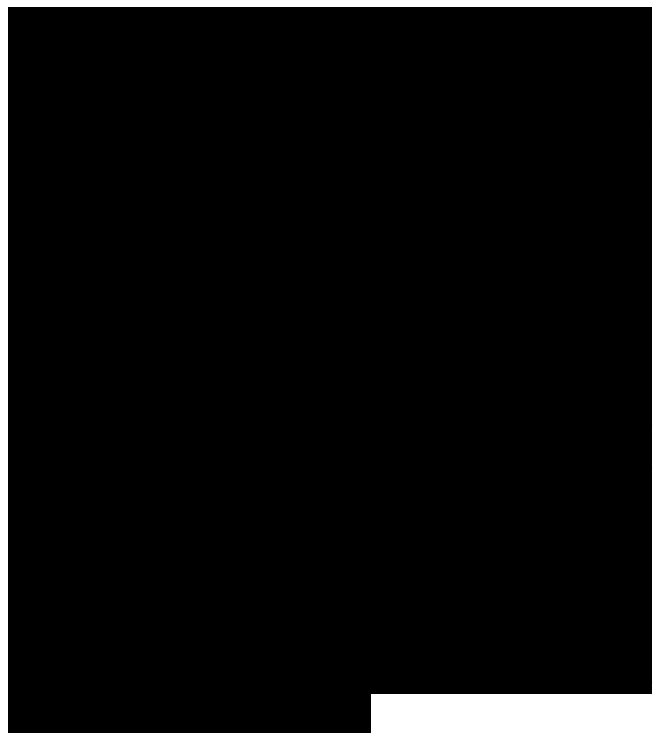
Chúng tôi trình bày kết quả thí nghiệm tán xạ tần số tổng trên hệ phân tán keo ở các nồng độ khác nhau và ở các cấu hình tán xạ khác nhau. Ở các góc tán xạ nhỏ, chúng tôi thấy có sự dao động mạnh mật độ photon tần số tổng tán xạ. Thông qua xem xét sự phụ thuộc góc của tín hiệu, sự phụ thuộc nồng độ hạt và phổ dao động bề mặt của hạt, chúng tôi kết luận rằng những dao động này là do hiệu ứng tán xạ từ các đám hạt. Hơn nữa, chúng tôi cũng chứng minh rằng hiệu ứng tán xạ ánh sáng phi tuyến động học có thể được dùng để đo kích thước của các đám hạt tương quan.



last 13 years, a rapidly growing number of publications reported on second-order Nonlinear Light Scattering (NLS) from small particles to probe their surfaces. Second-Harmonic Scattering (SHS) was used to probe (electronic) transitions on particle surfaces in condensed media [9-19] as well as liposomes in solution [20]. Vibrational Sum-Frequency Scattering (SFS) was performed to measure the molecular interface structure and its solvent dependence on colloids in solution [21-23], as well as inclusions in biodegradable polymer microspheres [24-26].

In such experiments, however, it is possible to induce competing incoherent nonlinear light scattering processes, such as Hyper-Rayleigh Scattering (HRS), Parametric Light Scattering (PLS), Two-Photon Fluorescence (TPF), and hyper-Raman scattering [27]. The energy schemes of these processes are illustrated in Fig. 1. In addition, a dispersion of colloids is a dynamic system in which particles can collide, aggregate, and diffuse. The effects of correlations from such processes have not yet been considered. Thus, a detailed understanding of the origins of these processes is crucial to the development and the rapid growth of diverse applications of NLS in various chemical and physical systems.

In this Article, we present sum-frequency spectroscopy scattering measurements performed in different geometries on dispersions with low and



high particle concentrations. By considering several coherent (SHS and SFS) and incoherent nonlinear light scattering (such as HRS, PLS, TPF) processes, we demonstrate that clusters can dramatically influence the signal at certain scattering angles. In addition, we show that using dynamic nonlinear light scattering, we can extract the size of the clusters. In Section II, we start with a theoretical background comparison between the various nonlinear light-matter interaction processes such as HRS, PLS, TPF, SHS and SFS, and consider their physical origins. In Section III, we discuss the experimental considerations such as laser parameters, experimental geometry, and sample preparation. In Section IV, we will use the discussion developed in Section II to explain our results and show that the observed angle-dependent intensity fluctuations can be explained by coherent scattering from particle clusters. We will then proceed with a demonstration of dynamic nonlinear light scattering, from which we evaluate the size of the clusters. Finally, the conclusion is presented in Section V.

- Sum Frequency Scattering (SFS)
- Second Harmonic Scattering (SHS)
- Parametric Light Scattering (PLS)
- Hyper Rayleigh Scattering (HRS)
- Two Photon Fluorescence (TPF)

FIG. 1: Schematic illustration of some common types of nonlinear light scattering. Coherent processes: Second-Harmonic Scattering (SHS), Sum-Frequency Scattering (SFS). Incoherent



processes: Hyper-Rayleigh Scattering (HRS), Parametric Light Scattering (PLS), Two Photon Fluorescence (TPF, Δ indicates an energy difference that could be zero) and hyper-Raman Scattering.

II. THEORETICAL

BACKGROUND: SCATTERING FROM ISOLATED PARTICLES IN SOLUTION

In this section, we will describe second-order nonlinear scattering from molecules in solution and on particle surfaces. We will assume that the incoming electric fields are plane waves of the form

where ω_1 and ω_2 are the angular frequencies, and k_1 and k_2 are the wave vectors. In general both coherent and incoherent scattering processes that lead to the emission of sum frequency photons with wave vector k_0 and frequency $\omega_1 + \omega_2 = \omega_0$ can take place. Coherent optical scattering refers to the electric field scattered from different locations arising from a superposition of nonlinear polarization sources that have a defined phase relation. Incoherent nonlinear scattering refers to additional radiation due to local fluctuations in the electric dipole moment that may arise from, e.g., dephasing or orientational fluctuation. Consequently for the coherent process, the radiated power scales as N^2 , whereas for the incoherent process, the power scales as N , where N is the number density of the dipole sources, e.g., molecules.

A. Incoherent nonlinear light

scattering from molecules in solution

From a historical point of view, the case of the incoherent second-order nonlinear optical scattering has been well studied beginning with the work of Terhune et al. [28] and further developed by others [29-34]. For a general three-photon scattering process arising from randomly oriented non-correlated (NC) molecules, (which includes PLS, HRS, TPF, as well as hyper-Raman scattering processes) the measured intensity (INC) can be expressed in the form

where t_a ($a=9$ or 0) is the component of the unit polarization vector e of the second-harmonic or sum-frequency signal detected along the r direction, A_{ai} is the element of the transformation matrix from the Cartesian reference frame to the polar coordinates reference frame, [28, 30, 31, 33, 34], p_{jk} is the molecular hyperpolarizability, and G is a constant quantity that depends on the geometrical parameters of the detection system. Note that all subscript indices refer to the laboratory frame. The angular brackets denote orientational averaging due to the random orientation of the molecules.

The various incoherent scattering processes have different polarization properties. Although their directionalities (radiation patterns) are also distinctive, in general scattered photons can appear in all directions. This can be seen directly from the term $(P_{ji}P_{mn})$, a six-ranked tensor, which governs the overall scattering process. For example, for a molecule having a

general symmetry, there is a maximum of 15 measurable quantities for PLS, which correspond to the number of the rotational invariants derived from the decomposition of the $(2) \otimes (2)^*$ tensor [31, 33, 34]. For a non-resonantly excited SF-TPF process, this number reduces to 7 [32]. These numbers of observables are further decreased when considering the corresponding light generating processes of HRS and SH-TPF. From these observations, these various processes have the potential to be uniquely identified based on their polarization properties and their radiation patterns. Another significant difference between these incoherent processes lies in their response time. In particular, PLS and HRS are instantaneous processes while the TPF is a delayed process. For the case of TPF, two-photon absorption occurs in a molecule, which later fluoresces from the same orientation and may occur at other frequencies. An intermediate relaxation to a fluorescing state may occur between these two effects (see Fig. 1). Thus in the TPF process, the total process may occur on a vibrational time scale but can also take much longer. Furthermore, the two-photon absorption and fluorescence are two independent quantum mechanical processes that do not interfere with each other. It should be noted that higher-order processes such as three-photon absorption and subsequent fluorescence might also contribute to the SH or SF signal [31].

Various schemes have been developed in order to distinguish between these

incoherent processes such as spectral separation [35], direct temporal separation [36], and temporal separation in the Fourier domain [37]. Polarization dependencies of the PLS [38] and HRS [39, 40] measurements have been demonstrated previously.

B. Coherent nonlinear light scattering from a particle

Here, we consider only molecules adsorbed on spherical particles (with radius a and refractive index n_1), because most materials consist of isotropic material and experiments on planar substrates have shown that very often the isotropic bulk response can be neglected. For coherent NLS from a non-isotropic bulk see e.g. Ref. [24]. For the case of a sphere, embedded in a medium with refractive index n_2 , the coherently emitted nonlinear signals arise from its surface because of the strong orientational correlation of the adsorbed molecules due to the selectivity of the molecular adsorption or binding process. There is a definite phase relationship between the dipole sources that are located at different locations and, as a consequence, this may give rise to coherent signal. At the surface of a particle, orientational correlation between neighboring molecules may give rise to an effective local nonlinear optical response, which may be described by the nonlinear surface susceptibility χ_S . Various theoretical formalisms of SHG and SFG from single spheres have been developed [21, 41–52]. The nonlinear polarization of the SF signal arising from molecules located

at the surface of a sphere is denoted by

(5)

The tensor quantity X^{\wedge} is related to the hyperpolarizability tensor $\wedge^{(2)}$ according to the equation [1]:

(6)

where N_s is the molecular surface density, T_{ia} is an element of the transformation matrix T that transforms from the molecular frame to the particle surface reference frame, and is an element of the hyperpolarizability tensor in the molecular frame. In reality, one needs to calculate the electric fields at the location of the dipole source r' as indicated in Eq. 5 prior to calculation of the nonlinear polarization $P^{(2)}(\wedge_i + u_2, r')$. After obtaining the nonlinear polarization, the relevant boundary conditions are applied [45], which then yield the SH or SF field $E(w_1 + w_2, r')$. The solution to the exact and general problem is outlined in Ref. [53] for SHS where it is applied to small particles in the Rayleigh limit and in [52], where it is applied for SFS using the principle of time reversal. Because of the sheer complexity of the problem, approximations such as the Rayleigh-Gans-Debye (RGD) [21, 43, 49, 50, 53-55], and Wentzel-Kramers-Brillouin (WKB) [49, 56] methods have been proposed. See Ref. [57] for an overview.

Here, we consider only the RGD method, which has been shown to work for silica particles in solution with radii up to 650 nm and a refractive index difference at the SF wavelength of 0.03 [21, 49]. Within the RGD model, the

internal field is assumed to be the same as the incident field. This model is roughly valid under two conditions: (1) $|m - 1| \ll 1$, where $m = n_1/n_2$ and (2) $4na|m - 1|/A \ll 1$, where A is the smaller of the two wavelengths corresponding to w_1 or u_2 . This model has been shown to be quite successful in describing the radiation patterns of SH and SF scattering from spherical particles. Fig. 2 shows an illustration of the experimental geometry and relevant parameters.

The coherent (C) contribution to the SF signal has the following form:

(7)

(2)

where r_{jk} is the effective susceptibility (see [49]) of the sphere together with the adsorbed molecules and G' is a constant that depends on the geometry of the detection system. Within the RGD model the effective susceptibility of a single vibrational or electronic transition can be expressed as

(8)

where we have the Cartesian lab frame coordinate system $e_{ij,k}$, the Cartesian coordinate system spanned by the scattering wave vector q , q_i , m, n and the spherical coordinate system (r', θ', ϕ') . The wave vector q and its magnitude are here defined as:

(9)

(10)

where k_0 is the wave vector of the scattered SF light and θ is the scattering angle. An inspection of Eq. 7 reveals that the coherent contribution to the SF signal



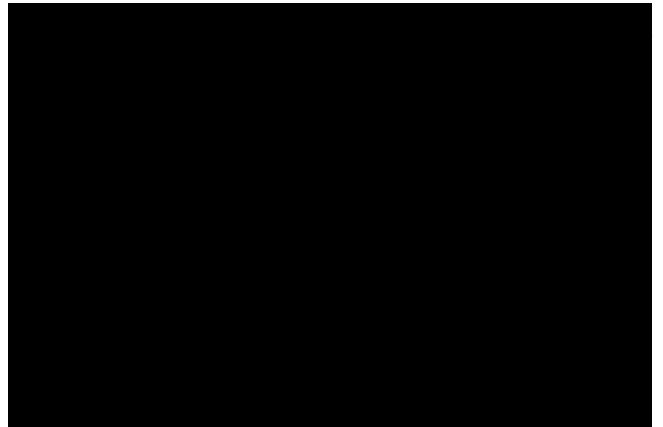
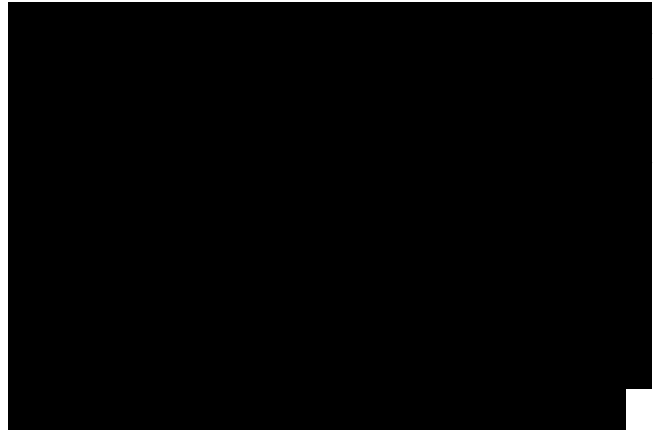
is governed by the 3-ranked tensor $r(2)$. We also see directly from Eq. 6 and 7 that the total coherent signal IC depends quadratically on particle surface density N_s . We further see from Eq. 8 that the coherent signal depends on the radius a of the particle. Furthermore the scattering signal vanishes for $q = 0$ (in the forward direction), which is identical to $\theta = 0$ (in the RGD approximation, see Fig. 2).

III. EXPERIMENTAL

The SFS experiments were performed using a 1 kHz amplified Ti:Sapphire amplifier which pumped an optical parametric generator/amplifier stage with a subsequent noncollinear

FIG. 2: Illustration of the in-plane scattering geometry of the experiments, indicating the k -vectors of the incoming beam (k_1 and k_2) and the scattered sum frequency beam k_0 , the scattering wave vector (q), and the scattering angle (θ). Beams polarized parallel to the plane of incidence are defined as p-polarized, while beams with an oscillating field in the y -direction are indicated as s-polarized. The direction $k_1 + k_2$ is called the forward direction ($\theta=0$).

difference frequency generation stage (TOPAS, Light Conversion) (see Ref. [21] for Figs. 3 -4 and Ref. [58] for Fig. 6). The pulse bandwidths and energies are given in the respective figure captions. The selectively p-polarized IR and VIS pulses were incident under a relative angle of 15° (fl) and focused down to a ~ 0.4 mm beam waist. The scattered light was collimated with a



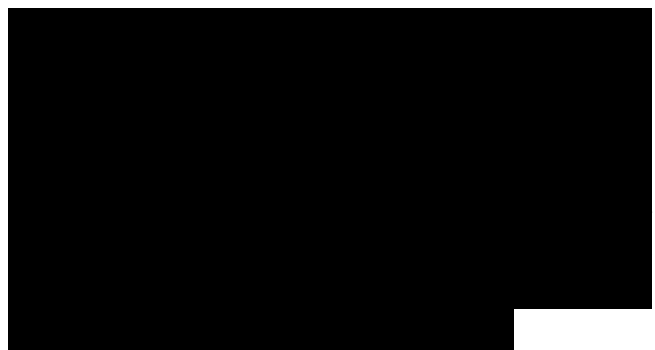
lens, p-polarization selected and dispersed onto an intensified charge coupled device (CCD) camera. The angular resolution was controlled by an aperture placed in front of the collimating lens. The samples consist of stearic alcohol (C₁₈H₃₇OH)-coated [59] silica particles [60] dispersed in CC₁₄ (99.9%, Baker Analyzed) with a radius $a = 342 \text{ nm} \pm 36 \text{ nm}$, as measured with Transmission Electron Microscopy (TEM) [21]. The colloid volume fractions was 5 or 25 v.v.%. The sample cell consists of 2 CaF₂ plates separated by a 1 mm teflon spacer. The scattering geometry is illustrated in Fig. 2.

IV. RESULTS AND DISCUSSION

We have performed vibrational SFS measurements on colloidal dispersions with short integration times and in different scattering angles, and observe strong fluctuations in the scattered intensity. We have investigated the effect of clustering further by increasing the colloid volume fraction from 5 v.v% to 25 v.v%.

A. Angular dependence

FIG. 3: Vibrational SFS spectra of a 5 v.v.% colloidal dispersion, measured with 10 (120 fs) IR pulses centered at 2900 cm⁻¹ and 3.0 J 800 nm visible (VIS) pulses with a 10 cm⁻¹ bandwidth, at a scattering angle of $\theta = 63^\circ$. (a) Image array of 100 spectra. The color scale indicates the intensity. (b) One 6 s spectrum (number 83). (c) The integrated intensity per spectrum. The angular

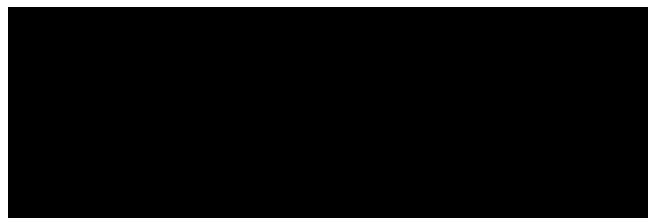


resolution was 12° .

contrast, in Fig. 4 the same type of experiment is shown except that the detection angle is closer to the forward direction at $\theta = 16^\circ$. Here, we observe large fluctuations ("hot spots") in the intensity as a function of time.

The observed intensity fluctuations can be due to coherent scattering from large objects, like clusters but also in principle due to incoherent light scattering. As described in section II, we can distinguish between these processes by analyzing the angular dependence of the signal and the spectral content. TPF of the double IR or VIS frequency typically occurs in a different frequency range, which makes it easily distinguishable. While it could be playing a role in similar SHS experiments, TPF does not occur in these SFS experiments since there are no electronic transitions that match any combination of incoming beams. PLS from the solution molecules can be a candidate for signal distortion because the radiation pattern for PLS is (like that of HRS) relatively isotropic. However, since the generation of PLS typically requires a large dipole moment [27, 38] it is not a likely source for the strong fluctuations that were observed. Since there was no signal from a neat solution we can exclude PLS as a source for scattering.

This means that the observed hot spots could come from a coherent surface scattering process. In order to get more insight into the source of the scattering we have analyzed the spectral features of



both the fluctuating high intensity and the constant low intensity signals. Fig. 5 (left panel) shows the average SFS spectrum of the hot spots present in Fig. 4, compared to the average spectrum of the constant low intensity signal. It can be seen that both the spectral intensity as well as the spectral shape are completely different. Spectral fits were made according to the well-known description of vibrational sum-frequency spectra, so that the spectral shape could be described by the following expressions (see e.g. [21, 61]):

(11)

where ANR refers to the angle dependent amplitude of the non-resonant background with relative phase A_0 , n refers to a vibrational mode, with resonance frequency ω_n , amplitude A_n and damping constant γ_n . Both the resonant and non-resonant amplitudes are angle dependent [57]. The averaged spectra of the small intensity signal can be attributed to single particles and could be fit with the resonances of the surface bound stearyl groups without assuming a non-resonant contribution. For the fit, both the symmetric CH₃ ($A_{2885} = 11-4$) and CH₂ stretch modes ($A_{2850} = 20-4$) and the asymmetric CH₂ ($A_{2911} = 14-6$) and CH₃ stretch ($A_{2972} = 2-16$) modes were needed as well as the Fermi resonance ($A_{2932} = 10-3$). These fits were almost identical to the ones presented in Ref. [21] and the presence of all these modes indicates that the surface chains are disordered (as was shown earlier [21, 22]).

The spectral signature of the averaged



hot spot spectrum (Fig. 5, upper trace) is remarkably different and could not be described without an appreciable amount of non-resonant background ($ANR = 2$, $A_0 = 100^\circ$). Additionally the symmetric CH2 and CH3 stretch amplitudes decreased with a factor of 2. The asymmetric CH3 and CH2 modes increased with a factor of 2 and 5 respectively, while the amplitude of the Fermi resonance changed very little.

These changes indicate that the source of the hot spot still has alkane chains attached to it, although the average conformational distribution is different. Thus, the object giving rise to hot spots are composed of dispersed colloids. Provided the non-resonant signal depends on the amount of bulk material in the object, the increase in non-resonant signal points towards an increase in bulk (silica) material. Further, we observe only hot spots when the scattering angle is in the range $\sim -30^\circ < \theta < 30^\circ$. Using Eqs. 7 and 8 we have calculated the scattering pattern within the RGD approximation for spheres with different sizes. Fig. 5 (right panel) shows calculated angular distributions (using the non-linear RGD model in combination with the parameters for stearyl-coated silica particles as

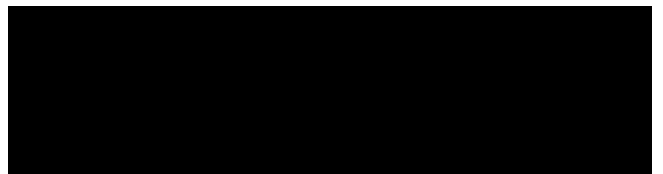
FIG. 5: Left: Averaged normal (single particle) spectra (red trace) and averaged hot spot (blue trace) taken at $d = 16^\circ$. The spectral shape as well as the intensity are remarkably different. The straight lines are fits to the data according to the description in the text.



The Lorentzian peaks indicate the five vibrational resonances described in the text used for the fitting. Right: Scattering patterns for dielectric particles with a surface response modelled according to the RGD approximation for ppp-polarization for different particle sizes. The angle between k_i and k_2 was 15° and the surface response was defined using the following parameters: $X_{\pm} \backslash \backslash \backslash X_{\pm \pm \pm} = -0.29$, $x_{fiw}/x_{fW} = 0.28$, and $X^{\wedge} J_{xfW} = 0.32$ [21].

obtained from [21]) of scattered SF photons for particles with different sizes (a , $10a$ and $100a$). It shows that large objects scatter preferentially in the forward direction and that the intensity of the large particles is much larger than that of a small particle, so that one scattering event from a big particle may easily overwhelm the signal of thousands of single particles. Thus, it seems that the hot spots originate from clusters composed of multiple aggregated particles. A similar intensity dependence with time has been observed for SHS from disk shaped montmorillonites with a diameter of 500 nm [11]. In this study, the hot spots were attributed to fluctuations due to rotational reorientation of single particles. Since we are dealing with spherical particles, we can exclude that reorientation of single particles attributes to the observed fluctuations.

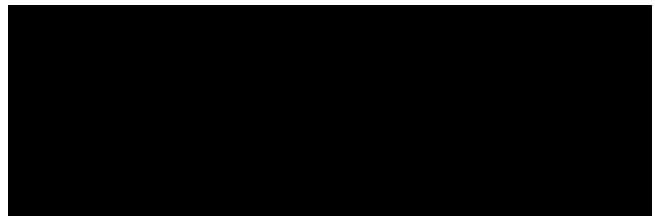
SHS performed under the same conditions would display similar intensity fluctuations and a similar angular distribution pattern. However,



SHS is mostly performed with adsorbed molecules (such as malachite green) that have a large hyperpolarizability tensor. Since these molecules are also in the solution, we can expect that they will be a source for incoherent light scattering as well (see Eq. 2). Thus, apart from SHS there might also be TPF and HRS. All three processes can emit at the SH wavelength in the forward direction. Although the selection rules for HRS, TPF, and SHS are different, it can be a complicated procedure to separate these processes from each other. In the case of SFS, vibrational charge oscillations are probed, so that the amplitude of the effective hyperpolarizability tensor from the solution would be expected to be very small compared with that of molecules from the particle and that the contribution from Eq. 2 will be below the detection limit.

Another type of emission may occur if the fundamental excites a longitudinal second-order polarization in the isotropic solution or bulk of the particle [62]. This contribution is expected to be a weak contribution, since it arises from a quadrupolar term. Because the spatial extent of vibrational wavefunctions are typically much smaller than that of electronic wavefunctions, the contribution of this quadrupole effect will be smaller for vibrational SFS than for SHS [63].

It therefore seems that while SFS has the possible drawback of being experimentally more involved than SHS, it has the advantage of having fewer competing incoherent processes. In



addition, the surface vibrational spectrum of the particles can be retrieved.

B. Dynamic nonlinear light scattering
In order to investigate the effect of cluster formation in the dispersion we have performed Dynamic Nonlinear Light Scattering (DNLS) of suspensions with different concentrations of colloids. To be more sensitive to the fluctuations we have sacrificed some spectral resolution by binning the chip of the CCD camera [64] with 10 pixels (a single spectrum is shown in the inset). The resultant recording time can then be reduced to 200 ms, so that a reasonable amount of statistics can be performed.

Fig. 6 (left panel) shows the result. Two series of integrated intensity are shown: one for a 5 v.v.% dispersion and one for a 25 v.v.% dispersion. Clearly, the intensity varies much more for the highly concentrated dispersion. In the case of the 5 v.v.% dispersion, the same low intensity signal appears most of the time, while sometimes a hot spot appears. With the 25 v.v.% concentration it is different. In addition to several hot spots there is also a signal that is persistently higher. The right panel of Fig. 6 displays the autocorrelations of both scattering signals. It can be seen that on the timescale of our measurement there is a fast decay in the 5 v.v.% dispersion. Our experiment resembles a dynamic light scattering

FIG. 6: Left: Integrated scattering



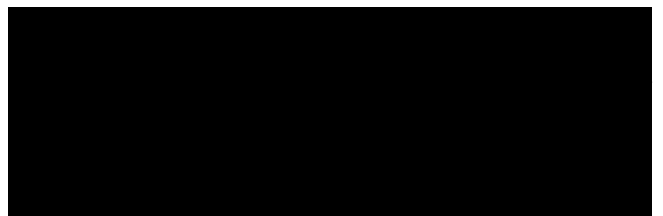
intensity as a function of time, t , obtained using 7 μJ (150 fs) IR pulses centered at 2895 cm^{-1} and 3.0 μJ , 800 nm visible (VIS) pulses with a 5 cm^{-1} bandwidth and measured at a scattering angle of 25° (with a resolution of 8°), for a 5 v.v.% dispersion of colloids (red) and a 25 v.v.% dispersion (black). Right: Corresponding autocorrelation traces of the SFG intensity for both dispersions over a time delay range of $0 < t < 150$ s. Right top panel: The same trace over a delay range of $0 < t < 2$ s and their exponential fits using Eq. 12.

experiment [65, 66], with a very low time resolution. This means we cannot observe the diffusion of single particles, but we should be able to observe diffusion of large objects, such as clusters. In the limit that self-diffusion is the dominating factor in the total diffusion of such clusters, the time autocorrelation function can be described by [65]:

$$(12)$$

where A is an amplitude factor, t is the autocorrelation time, and q represents the scattering wave vector (see Eq. 10). We can now fit the decaying part of autocorrelation of the 5 v.v.% dispersion with Eq. 12. For the diffusion constant D , we find that it lies in the range $7 \cdot 10^{-15} < D < 5 \cdot 10^{-14} \text{ m}^2/\text{s}$.

Using the Einstein diffusion model to obtain a first indication of the radius (a) of the object, we have $a = \sqrt{k_B T / 6 \pi \eta D}$, with the temperature T , ($T=293$ K), and the viscosity η ($\eta = 0.908 \text{ mPa} \cdot \text{s}$).



For the given values of D we find that the corresponding radius of the cluster size is $4.4 < a < 45$ fm. This range is consistent with our above description and matches roughly the size of the clusters that would be needed to generate hot spots (see Fig. 5, right panel) in an angular distribution close to the forward direction. In addition, the signal intensity from these clusters is comparable to that generated by an ensemble of single particles in the laser focus. It should be noted, however, that the agglomerates are probably not spherical and that there may be a different angular dependence for nonlinear light scattering compared to linear light scattering. That we can describe our data with the simple exponential expression indicates that the above description is correct, at least for a first-order approximation.

Fig. 6 also displays the DNLS results of a 25 v.v.% dispersion. The time scale of diffusion of clusters (0 - 2 s) is enlarged in the upper trace. It can be seen that for short time delays T the decay of the data can be described with an exponential decay similar to the DNLS result of the more dilute dispersion. For longer time delays there is a slow decay and a minimum occurs at ~ 70 s (see the arrow). Clearly, we cannot describe this behavior anymore with single particle or even cluster diffusion. Oscillations [67] and non-exponential decay [68] have been observed in linear DLS measurements. Their origin is not always clear, because a number of factors may influence the result. These factors include the following: scattering from

bubbles generated by laser heating [69], multiple scattering, local correlations between particles [68], cluster growth due to instability [70], electric field induced changes in the viscosity [71], the existence of different species having different scattering powers and density fluctuations in the sample [67]. Since there is no appreciable absorption of either the infrared or the visible laser pulse we can exclude the scattering from bubbles. Multiple scattering is suppressed in SHS and SFS with respect to linear light scattering because:

(i) the interaction volume of the pulses is small which reduces the scattering volume, (ii) the scattering efficiency is much smaller and (iii) the contrast is determined by $\langle x^2 \rangle$ instead of $\langle X \rangle$. For these reasons we believe that while linear light scattering can be used only at low volume fractions (of typically 0.1 v.v.% [59]), SHS and SFS can be applied at much higher volume fractions. This also means that linear light scattering cannot be used to clarify our observations and indeed we were not able to perform DLS measurements on these samples.

The other effects however can all contribute and a combination of those may give rise to the complex behavior observed in Fig. 6. One possible experiment to further investigate nonlinear light scattering from dense colloidal dispersions could be to measure the nonlinear scattering of the visible beam in an SHS scattering experiment as

well as the scattered light of the sum frequency process simultaneously in a dynamic light scattering experiment. The cross-correlation of the time dependent intensities will be free of any contributions from multiple scattering [72].

V. CONCLUSIONS

We presented sum-frequency scattering measurements performed in different geometries on dispersions with low and high particle concentrations. These measurements display high intensity fluctuations. From angle dependent spectrally resolved sum-frequency scattering measurement, the calculation of scattering patterns and concentration dependent dynamic nonlinear light scattering measurements we were able to determine that the high intensity fluctuations are due scattering from particle clusters.

Clustered colloids scatter with much higher intensities in angles close to the forward direction. The surface structure of the clusters is different from the single particle surface structure. From dynamic nonlinear light scattering experiments we have determined that the cluster size ranges from several tens to thousand times the single particle radius. In this size range the signal of one cluster can be comparable to that of thousands of single particles.

We have therefore clarified a number of effects that can considerably complicate (the interpretation of) nonlinear light scattering experiments. With this study, we hope to pave the way for investigations of the interface structure

V. KẾT LUẬN

Chúng tôi trình bày kết quả các phép đo tán xạ tần số tổng ở các cấu hình khác nhau trên các huyền phù ở nồng độ hạt thấp và cao. Qua những phép đo này chúng ta thấy có sự dao động nồng độ mạnh. Từ phép đo tán xạ tần số tổng phân giải phổ phụ thuộc góc, tính toán kiểu tán xạ và các phép đo tán xạ ánh sáng phi tuyến động học phụ thuộc nồng độ, chúng tôi thấy rằng sự dao động nồng độ bắt nguồn từ các đám hạt.

Chất keo kết tụ tán xạ theo góc gần với hướng tới nhiều hơn. Cấu trúc bề mặt của đám hạt khác với cấu trúc bề mặt của từng hạt. Từ thí nghiệm tán xạ ánh sáng phi tuyến động học, chúng tôi khẳng định rằng khoảng kích thước của đám hạt lớn hơn vài chục đến hàng nghìn lần bán kính từng hạt. Trong khoảng kích thước này, tín hiệu của một đám hạt tương đương kích thước của hàng nghìn hạt đơn lẻ.

Do đó chúng tôi đã làm rõ một số hiệu ứng có thể làm phức tạp đáng kể (giải thích) các thí nghiệm tán xạ ánh sáng phi tuyến. Thông qua nghiên cứu này, chúng tôi hy vọng sẽ tạo tiền đề cho các nghiên cứu cấu trúc bề mặt phân cách và động học của các

and the kinetics of interface processes in soft matter dispersions such as, colloids, emulsion and vesicles.

quá trình ở bề mặt phân cách trong các chất huyền phù mềm chẳng hạn như keo, nhũ tương và các lỗ hổng.